CHAPTER 2

CHARACTERIZATION AND OPTIMIZATION OF THE CMP PROCESS

In the Chemical Mechanical Polishing (CMP) process used for microelectronics manufacturing, three contact regimes between the wafer surface and the polishing pad may be proposed: direct contact, mixed or partial contact, and hydroplaning. An effective *in-situ* method for characterizing the wafer/pad contact and a systematic way of relating contact conditions to the process parameters are both lacking. In this work, the interfacial friction force, measured by a load sensor on the wafer carrier, characterizes the contact conditions. Models that relate the friction coefficient to the applied pressure, relative velocity, and slurry viscosity are developed and verified by experiments. Additionally, a correlation between friction coefficient and the material removal rate (MRR) is established. The effects of process parameters on the Preston constant are investigated. Process optimization methods based on extending the high-material-removal regime are also suggested and discussed.

2.1 Introduction

The ever-increasing demand for high-performance microelectronic devices has motivated the semiconductor industry to design and manufacture Ultra-Large-Scale Integrated (ULSI) circuits with smaller feature size, higher resolution, denser packing, and multi-layer interconnects. The ULSI technology places stringent demands on global planarity on the Interlevel Dielectric (ILD) layers. Compared with other planarization techniques, the Chemical Mechanical Polishing (CMP) process produces excellent local and global planarization at low cost. It is thus widely adopted in many back-end processes for planarizing inter-level dielectric (SiO_2) layers. In addition to achieving global planarization, CMP is also critical to many emerging process technologies, such as the polishing of Cu

damascene patterns, low-k dielectrics, and shallow trench isolation (STI) (Landis et al., 1992; Peters, 1998). The wide range of materials to be polished concurrently or sequentially, however, increases the complexity of CMP and necessitates an understanding of the process fundamentals for optimal process design and control.

Despite its extensive use in ULSI manufacturing, the basic material removal mechanisms in CMP are not yet well understood. Long ago, Preston empirically found in glass polishing that the material removal rate (MRR) is proportional to the product of the applied pressure and the relative velocity (Preston, 1927). The Preston equation may be written as:

$$\frac{d\xi}{dt} = k_p p v_R \tag{2.1}$$

where ξ is the thickness of the layer removed, t the polishing time, p the nominal pressure, v_R the relative velocity, and k_p a constant known as the Preston constant.

In recent years, many works have demonstrated that the above relation is also valid for metals (Steigerwald et al., 1994; Stavreva et al., 1995 and 1997) and ceramics (Nakamura et al., 1985; Komanduri et al., 1996). To explain this proportionality, several researchers proposed particle abrasion (Brown et al., 1981; Liu et al., 1996) and pad asperity contact models (Yu et al., 1993) to elucidate the mechanical aspects of the CMP process. Assuming that wafer/abrasive or wafer/pad is in contact, the applied stress field near the wafer surface results in elastic-plastic deformation of the surface layer and produces wear. Another line of research focused on the chemical mechanisms of the process (Cook, 1990; Luo et al., 1998). Cook first reviewed the chemical process for glass polishing. He suggested that both surface dissolution under particle impact and the absorption or dissolution of wear particles onto the slurry particles will determine the polishing rate of glass. More recently, a two-dimensional wafer-scale model based on lubrication theory (Runnels and Eyman, 1994) and mass transport was proposed (Sundararajan et al., 1999). In this model, the wafer is assumed to hydroplane on the pad surface, and the normal load is supported by the hydrodynamic pressure of the viscous slurry film. The polishing rate is determined by the convective mass transport of the chemical species.

Whether CMP material removal is by mechanical, chemical, or chemomechanical interactions, understanding the contact condition at the wafer/pad interface is crucial to process characterization, modeling, and optimization. However, to date there is no explicit methodology in the CMP literature to characterize wafer-scale interfacial conditions with process parameters. Some researchers assumed that the wafer hydroplanes while being polished. They solve the Reynolds equation of lubrication to determine the relations among wafer curvature, applied pressure, relative velocity, slurry viscosity, slurry film thickness, and pressure distribution on the wafer surface (Runnel, 1994; Runnel and Eyman, 1994). Another group assumed the wafer is in contact, or partially in contact with the pad. They relate the displacement of the wafer to the pad elastic modulus and solve the stress field by the classical contact mechanics model (Chekina et al., 1998). Measurement of the vertical displacement of the wafer relative to the pad seems the most direct way of identifying the contact condition and determine the slurry film thickness (Mess et al., 1997). However, the compliance of the pad material and the back film in the wafer carrier make such measurements unreliable. While some experiments in the hydroplaning mode were conducted on smaller specimens (Nakamura et al., 1985), scaling up the results to a larger size wafer is problematic. In general, different applied pressure, velocity, and other experimental conditions employed by various investigators result in difficulty in drawing any definitive conclusions regarding the mode of interfacial contact.

This chapter, accordingly, proposes a systematic way of characterizing and monitoring the wafer/pad interfacial condition. It also establishes a theoretical framework for relating the process parameters to the different contact modes is established. Polishing experiments were conducted on Cu blanket wafers to verify the analysis. The results are shown in a parametric form. Thus, the characterization technique is not limited to Cu blanket wafer polishing. Optimization of the process for a stable interfacial condition and the design of a robust CMP process for reducing wafer-scale variation can be based on this study.

2.2 Theory

2.2.1 Interfacial Contact Conditions. When a wafer is pressed against the polishing pad and slides with an intervening fluid layer, the polishing slurry, interfacial conditions can be characterized as: contact, hydroplaning and mixed mode. Figure 2.1 shows the schematics of these three modes. In the contact mode, the asperities of opposing surfaces (wafer/pad or wafer/particle) interact mechanically. The real contact area is usually much smaller than the nominal surface area. Plastic deformation occurs on both surfaces at the contact spots. The intervening fluid film is discontinuous and no significant pressure gradient is formed in the fluid film across the diameter of the wafer to support the normal load. This type of contact mode occurs in the CMP practice when the relative velocity is low or the applied pressure is high. The friction coefficient is relatively higher than that of the other two modes, usually on the order of 0.1 because a tangential force is required to shear the surface asperities,.

In contrast, when the velocity is high or the applied pressure is sufficiently low, the wafer will glide on a fluid film without directly touching the pad. Because there is no surface contact, frictional force is due to the shear of the viscous fluid film. The friction coefficient is expected to be much smaller, in the range 0.001 to 0.01, for typical hydroplaning conditions. Pressure builds up in the viscous fluid film to support the normal load on the wafer. The pressure gradient is very sensitive to the wafer attack angle. A slight change of the attack angle, an unsteady slurry flow, or a partial wafer/pad contact due to mechanical vibration, may result in a shift away from the hydroplaning mode even if the velocity and the normal pressure requirements are satisfied.

The mixed mode is a transition from the contact mode to the hydroplaning mode. It occurs when velocity increases or pressure reduces. In this regime, the velocity is neither high enough nor the pressure low enough to build up a thick fluid layer to support the normal load. This results in some contact between the pad asperities and the wafer surface. The friction force is the weighted sum of the force necessary to deform the surface asperities at the wafer/pad and wafer/particle contacts and the shear of the viscous slurry film. The friction coefficient is usually between 0.01 and 0.1. The friction coefficient can be used as an

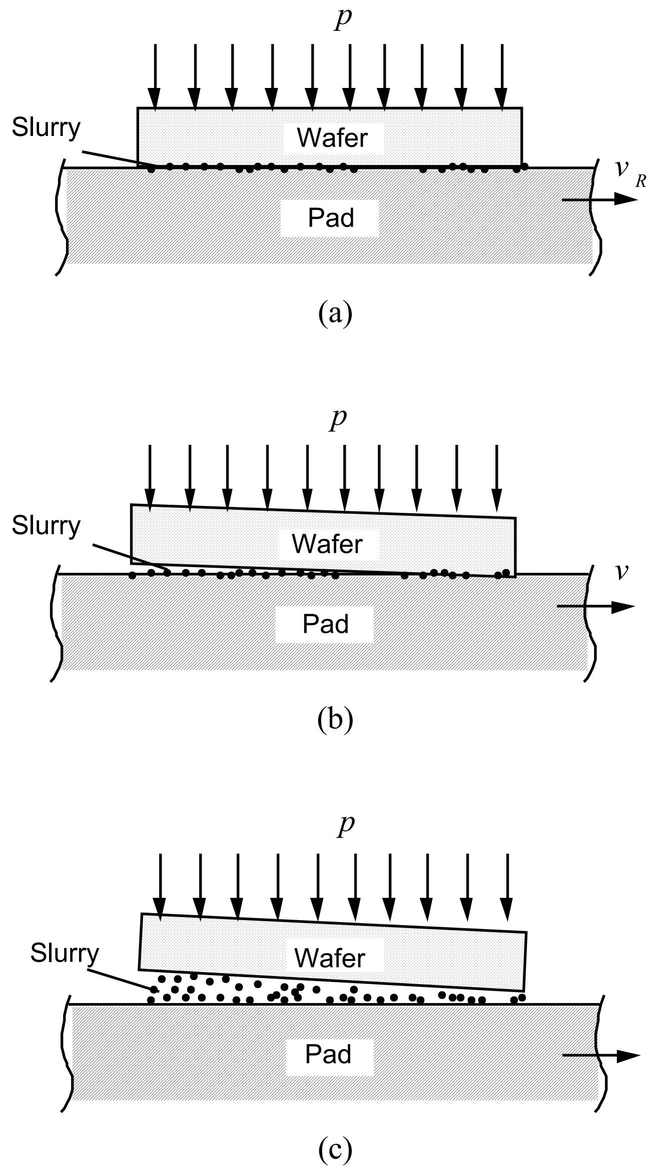

Figure 2.1 Schematics of the wafer/pad interface at (a) contact mode, (b) mixed mode, and (c) hydroplaning mode.

indicator of the wafer/pad contact conditions because it will vary by one to two orders of magnitude among the different contact modes.

2.2.2 Kinematics of Polishers. Current CMP practice uses both linear and rotary polishers. To analyze the kinematics, the coordinate systems for both types of polishers are shown in Fig. 2.2.

The pad, in the linear polisher, moves in the *x*-direction with a constant velocity v_p, and the wafer rotates at an angular velocity, ω_w, about its center O_w. The velocity components for the wafer, $v_{r,w}$ *and* $v_{\theta,w}$, and the pad, $v_{r,p}$ *and* $v_{\theta,p}$, in r, θ coordinates can be expressed as:

$$v_{r,w} = 0 \ ; \ v_{\theta,w} = \omega_w r \tag{2.2a}$$

$$v_{r,p} = v_p \cos\theta \ ; \ v_{\theta,p} = -v_p \sin\theta \tag{2.2b}$$

Therefore, the components of the relative velocity of the wafer to the pad are given as:

$$v_{r,R} = -v_p \cos\theta \tag{2.3a}$$

$$v_{\theta,R} = \omega_w r + v_p \sin\theta \tag{2.3b}$$

and the magnitude of the relative velocity can be written as:

$$\begin{aligned} v_R(r,\theta) &= [(v_p \cos\theta)^2 + (\omega_w r + v_p \sin\theta)^2]^{1/2} \\ &= [v_p^2 + 2\omega_w v_p r \sin\theta + \omega_w^2 r^2]^{1/2} \end{aligned} \tag{2.4}$$

In steady state, the average of the relative velocity components of points located at a radius r can be expressed as:

$$\bar{v}_{r,R} = \frac{1}{2\pi}\int_0^{2\pi} v_{r,R}\, d\theta = 0 \tag{2.5a}$$

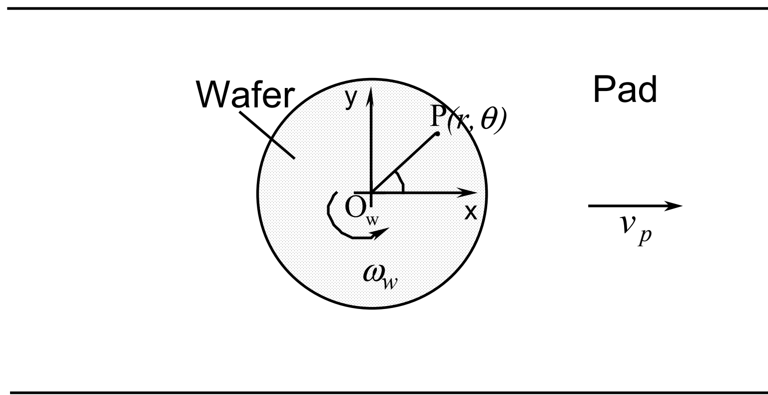

(a)

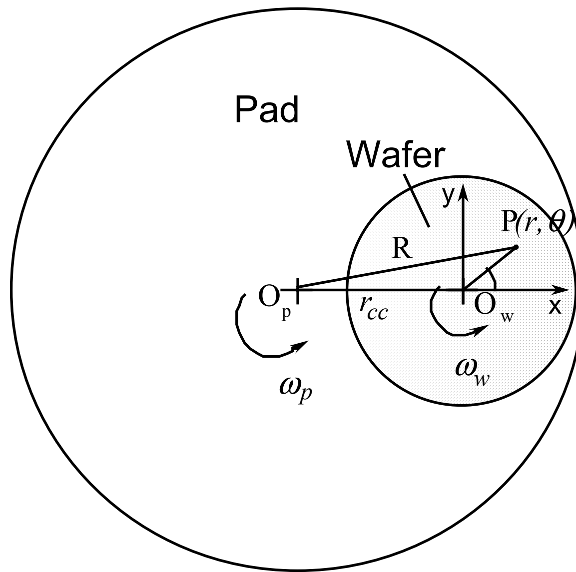

(b)

Figure 2.2 Schematics of coordinate systems for (a) linear and (b) rotary CMP processes.

$$\bar{v}_{\theta,R} = \frac{1}{2\pi}\int_0^{2\pi} v_{\theta,R}\, d\theta = \omega_w r \qquad (2.5b)$$

Equations (2.5a) and (2.5b) state that the wafer rotation provides isotropic polishing by the change of sliding direction at any point. However, if the circumferential velocity of the wafer is comparable to the pad velocity, the sliding distances for any point on the wafer will increase with the radius, which results in nonuniform wafer polishing. To reduce nonuniform polishing, the angular velocity of the wafer from Eq. (2.3b) must satisfy the inequality:

$$\omega_w << v_p / \mathrm{r_w} \qquad (2.6)$$

For the rotary polisher shown in Fig. 2.2 (b), the rotational centers of the wafer and the platen are O_w and O_p, and the angular velocities are ω_w and ω_p, respectively. The two rotational axes are normal to the polishing surface with an offset r_{cc}. The velocity components of the wafer at a point $P(r,\theta)$ are the same as in Eq. (2.2a). Those of the pad can be expressed as:

$$v_{r,p} = \omega_p r_{cc} \sin\theta \;\; ; \;\; v_{\theta,p} = \omega_p (r + r_{cc}\cos\theta) \qquad (2.7)$$

Therefore, the components of relative velocity, $v_{r,R}$ *and* $v_{\theta,R}$, can be written as:

$$v_{r,R} = -\omega_p r_{cc} \sin\theta \;\; ; \;\; v_{\theta,R} = \omega_w r - \omega_p (r + r_{cc}\cos\theta) \qquad (2.8)$$

The magnitude of the relative velocity is given as:

$$\begin{aligned} v_R &= [(\omega_p r_{cc}\sin\theta)^2 + (\omega_w r - \omega_p r_{cc}\cos\theta - \omega_p r)^2]^{1/2} \\ &= \{[(\omega_w - \omega_p) r \sin\theta]^2 + [(\omega_w - \omega_p) r\cos\theta - \omega_p r_{cc}]^2\}^{1/2} \end{aligned} \qquad (2.9)$$

By replacing $r\cos\theta$ and $r\sin\theta$ with x and y, v_R can be rewritten in the Cartesian coordinate system as:

$$v_R = \{[(\omega_w - \omega_p)y]^2 + [(\omega_w - \omega_p)x - \omega_p r_{cc}]^2\}^{1/2} \tag{2.10}$$

with the relative velocity components, $v_{x,R}$ and $v_{y,R}$, given by:

$$v_{x,R} = -(\omega_w - \omega_p)y \; ; \; v_{y,R} = (\omega_w - \omega_p)x - \omega_p r_{cc}$$

(2.11)

When the angular velocities of the wafer and the platen are equal, i.e., $\omega_w = \omega_p$, Eq. (2.11) can be simplified:

$$v_x = 0 \; ; \; v_y = \omega_p r_{cc} \tag{2.12}$$

Thus, the velocity of the wafer relative to the pad is in the y-direction and is identical at all points on the wafer. If the angular velocities of the wafer and the platen, $\omega_w = \omega_p$, and the distance between two rotational centers, r_{cc}, do not vary with time, the relative velocity will remain constant throughout the polishing process and always in the *y*-direction, but the direction will vary at a frequency of $\omega_w/2\pi$. This results in isotropic polishing. This setting will be used in the following analysis of interfacial condition and for process design, because a uniform velocity simplifies the analysis and, as will be discussed later, reduces the variation in material removal across the wafer.

2.2.3 The Contact Mode. By assuming Coulomb friction in the contact mode, the *x*- and *y*-components of the traction force acting on an infinitesimal surface element $\delta A = r\delta r\delta\theta$ of the wafer in the Cartesian/polar coordinate systems are given by:

$$dF_x = \frac{\mu p(r\delta r\delta\theta)[(\omega_w - \omega_p)r\sin\theta]}{\{[(\omega_w - \omega_p)r\sin\theta]^2 + [(\omega_w - \omega_p)r\cos\theta - \omega_p r_{cc}]^2\}^{1/2}} \tag{2.13a}$$

$$dF_y = \frac{-\mu p(r\delta r\delta\theta)[(\omega_w - \omega_p)r\cos\theta - \omega_p r_{cc}]}{\{[(\omega_w - \omega_p)r\sin\theta]^2 + [(\omega_w - \omega_p)r\cos\theta - \omega_p r_{cc}]^2\}^{1/2}} \tag{2.13b}$$

where μ is the Coulomb friction coefficient and p is the pressure on the surface element. At any point on the wafer, the direction of the friction force is the same as that of the direction of the resultant relative velocity. The x- and y-direction components of the frictional force on the wafer, F_x and F_y can be obtained by integrating Eqs. (2.13a) and (2.13b):

$$F_x = \int_0^{r_w}\int_0^{2\pi} \frac{\mu p(\omega_w - \omega_p) r^2 \sin\theta}{[\omega_p^2 r_{cc}^2 + (\omega_w - \omega_p)^2 r^2 - 2\omega_p(\omega_w - \omega_p) r_{cc} r \cos\theta]^{1/2}} d\theta dr$$
$$= 0 \qquad (2.14a)$$

$$F_y = \int_0^{r_w}\int_0^{2\pi} \frac{\mu p[\omega_p r_{cc} r - (\omega_w - \omega_p) r^2 \cos\theta]}{[\omega_p^2 r_{cc}^2 + (\omega_w - \omega_p)^2 r^2 - 2\omega_p(\omega_w - \omega_p) r_{cc} r \cos\theta]^{1/2}} d\theta dr \qquad (2.14b)$$

The x-direction force component, F_x, is always zero for all ω_w and ω_p because the x-direction differential force component, dF_x, in Eq. (13a) at (r, θ) is canceled by that at (r, 2π-θ). Thus, the frictional force in contact mode acts on the wafer in the y-direction only. The torque exerted on the wafer, Q_w, is given by:

$$Q_w = \int_0^{r_w}\int_0^{2\pi} \frac{\mu p r[\omega_p r_{cc} r \cos\theta - (\omega_w - \omega_p) r^2]}{[\omega_p^2 r_{cc}^2 + (\omega_w - \omega_p)^2 r^2 - 2\omega_p(\omega_w - \omega_p) r_{cc} r \cos\theta]^{1/2}} d\theta dr \qquad (2.15)$$

Similarly, the torque on the platen, Q_p, can be obtained as:

$$Q_p = \int_0^{r_w}\int_0^{2\pi} \frac{\mu p r[-\omega_p r_{cc}^2 + (\omega_w - 2\omega_p) r_{cc} r \cos\theta + (\omega_w - \omega_p) r^2]}{[\omega_p^2 r_{cc}^2 + (\omega_w - \omega_p)^2 r^2 - 2\omega_p(\omega_w - \omega_p) r_{cc} r \cos\theta]^{1/2}} d\theta dr \qquad (2.16)$$

Again, when $\omega_w = \omega_p$ and the pressure is uniform, Eqs. (2.14) to (2.16) reduce to:

$$F_y = \mu p_{ave} \pi r_w^2 \; ; \quad Q_w = 0 \; ; \quad Q_p = \mu p \; \pi r_w^2 r_{cc} \qquad (2.17)$$

The torque on the wafer vanishes. The friction coefficient μ, the ratio of tangential force F_t to the normal force F_n on the wafer, in the contact mode simplifies to:

$$\mu = \frac{F_t}{F_n} = \frac{F_y}{p_{ave}\pi r_w^2} \tag{2.18}$$

The *y*-direction force on the wafer carrier can be directly measured and the friction coefficient can be readily determined for the $\omega_w = \omega_p$ condition. Based on Eq. (2.17), the friction coefficient at $\omega_w = \omega_p$ condition can also be determined by the torque measurement on the platen, Q_p, and expressed as:

$$\mu = \frac{Q_p}{p\pi r_w^2 r_{cc}} \tag{2.19}$$

The above analysis is assumed that the wafer is not slipping, i.e., the wafer rotates at the same speed as the wafer carrier. If the wafer slips inside the carrier recess, however, the resulting non-uniform velocity distribution produces both the x-direction force and torque on the wafer as indicated by Eqs. (2.14) to (2.16). Since nonuniform velocity directly results in nonuniform polishing, the x-force and the wafer torque can be monitored during polishing to detect wafer slippage and to ensure polishing uniformity.

The friction coefficient in the contact mode may be affected by the materials of the wafer and the pad, their surface topographies, the presence of abrasive particles, and the chemical composition. But, to a first approximation, the Coulomb friction coefficient is independent of the applied normal load, the relative velocity, the slight bowing or warping of the wafer, and the viscosity of the slurry fluid.

2.2.4 The Hydroplaning Mode. Figure 2.3 is a schematic of a hydroplaning wafer with the gimbal mechanism at the center of the wafer carrier. In this mode, the normal load is not supported by the pad asperities or the abrasive particles, but by the pressure in the slurry fluid film. The differential equation governing the pressure distribution in the fluid

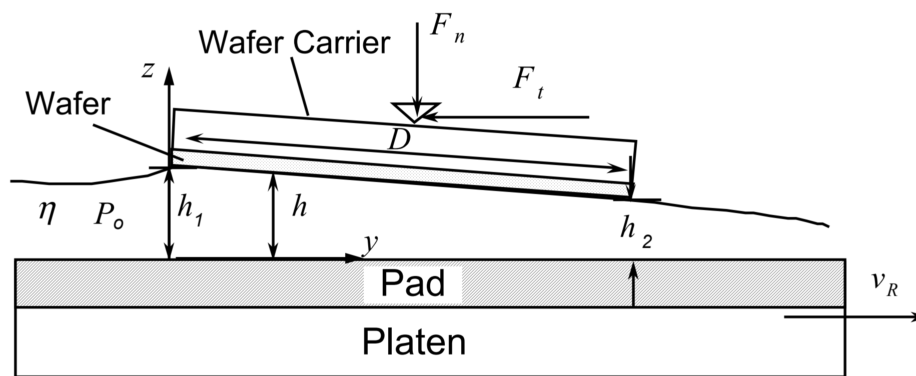

Figure 2.3 Schematic of wafer/pad interface in the hydroplaning mode.

film is known as the Reynolds equation. The derivation of the Reynolds equation from the Navier-Stokes equations and the continuity equation for Newtonian fluid and steady-state velocity field is available in the hydrodynamic lubrication literature (e.g., Hamrock, 1994). This derivation assumes a thin slurry film condition, i.e., $h_o/D << 1$, where h_o is a characteristic slurry film thickness and D is the wafer diameter. The two-dimensional Reynolds equation corresponding to the boundary velocity conditions in CMP may be expressed as:

$$\frac{1}{12\eta}[\frac{\partial}{\partial x}(h^3\frac{\partial p}{\partial x})+\frac{\partial}{\partial y}(h^3\frac{\partial p}{\partial y})]=\frac{\partial}{\partial x}[\frac{h(u_{x,w}+u_{x,p})}{2}]+\frac{\partial}{\partial y}[\frac{h(u_{y,w}+u_{y,p})}{2}]$$
$$+(u_{z,w}-u_{z,p})-(u_{x,w}\frac{\partial h}{\partial x}+u_{y,w}\frac{\partial h}{\partial y}) \qquad (2.20)$$

where h is the slurry film thickness, p the pressure, and η the slurry viscosity. With the subscripts w and p for the wafer and the pad, $u_{x,w}$, $u_{y,w}$, and $u_{z,w}$, and $u_{x,p}$, $u_{y,p}$, and $u_{z,p}$ are the velocity components of the wafer and the pad in the x, y, and z directions, respectively. (h, p, u, v, and w are functions of x and y only.) The physical interpretation of Eq. (2.20) is as follows. The two terms on the left-hand side represent the slurry net flow rate due to the pressure gradient. The first two terms on the right-hand side are the net slurry flow rate due to the drag from the motion of the wafer and pad surfaces. The last two terms, generally known as squeeze film terms, are the flow rates due to the relative z-direction motion of the wafer and pad surfaces.

Equation (2.20) can be rewritten for the rotary CMP polisher by substituting the velocity boundary conditions, $u_{x,w}$, $u_{y,w}$, $u_{x,p}$, and $u_{y,p}$, on the wafer and the pad surfaces given in the kinematics section:

$$\frac{1}{12\eta}[\frac{\partial}{\partial x}(h^3\frac{\partial p}{\partial x})+\frac{\partial}{\partial y}(h^3\frac{\partial p}{\partial y})]=\frac{(\omega_w-\omega_p)y}{2}\frac{\partial h}{\partial x}$$
$$-\frac{[(\omega_w-\omega_p)x-\omega_p r_{cc}]}{2}\frac{\partial h}{\partial y}+(u_{z,w}-u_{z,p}) \qquad (2.21)$$

At the condition $\omega_w = \omega_p$ and assuming no z-direction motion of the wafer or the pad, Eq. (2.21) reduces to:

$$\frac{1}{12\eta}[\frac{\partial}{\partial x}(h^3\frac{\partial p}{\partial x})+\frac{\partial}{\partial y}(h^3\frac{\partial p}{\partial y})]=\frac{\omega_p r_{cc}}{2}\frac{\partial h}{\partial y} \quad (2.22)$$

The boundary condition for solving Eq. (2.22) is that the pressure at the periphery of the wafer is zero:

$$p(x,y)=0 \quad \text{at} \sqrt{\mathrm{x}^2+y^2}=r_w \quad (2.23)$$

However, it is difficult to obtain an analytical solution for Eq. (2.22) with the boundary condition Eq. (2.23). If the point of the exercise is to study the qualitative behavior of the hydroplaning condition, a one-dimensional simplification of this problem is instructive. With the assumption that the "side-leakage" flow in the x-direction can be neglected, a simplified one-dimensional Reynolds Equation is obtained from Eq. (2.22):

$$\frac{d}{dy}(h^3\frac{dp}{dy})=6\eta v_R\frac{dh}{dy} \quad (2.24)$$

Integrating Eq. (2.24) and rewriting:

$$\frac{dp}{dy}=6\eta v_R\frac{h-h_o}{h^3} \quad (2.25)$$

where h_o is the film thickness at which the pressure gradient dp/dy is zero. This equation states the effects of process variables, i.e., slurry viscosity, relative velocity, and film profile, on the pressure gradient.

To solve Eq. (2.25), boundary conditions of the pressure at the inlet ($y = 0$) and outlet ($y = D$) will be employed; the origin is now at the inlet of the slurry film. Thus:

$$p(0) = 0 \text{ and } p(D) = 0 \tag{2.26}$$

By further assuming a planar wafer surface, the slurry film thickness h in Eq. (2.25) is expressed as:

$$h = h_1 - \frac{(h_1 - h_2)}{D} y \tag{2.27}$$

where h_1 and h_2 are the film thicknesses at the inlet and outlet and D is the diameter of the wafer. Using Eqs. (2.26) and (2.27), the pressure in Eq. (2.25) is:

$$p(y) = \frac{6\eta v_R (h_1 - h_2)(1 - y/D)y}{(h_1 + h_2)[h_1 - (h_1 - h_2)y/D]^2} \tag{2.28}$$

The normal load per unit width of the wafer in the x-direction, f_n, that the slurry film can support is obtained by integrating the pressure function from inlet to outlet. Thus:

$$f_n = \frac{6\eta v_R D^2}{(h_1 - h_2)^2} \left[\ln\left(\frac{h_1}{h_2}\right) - \frac{2(h_1 - h_2)}{(h_1 + h_2)} \right] \tag{2.29}$$

Additionally, the location of the pressure center, y_{cp}, is calculated by the expression:

$$f_n \, y_{cp} = \int_{-r_w}^{r_w} p y dy \tag{2.30}$$

Substituting Eq. (2.28) into Eq. (2.30), the center of pressure is obtained as:

$$y_{cp} = \frac{6\eta v_R D^2}{f_n \, (h_1^2 - h_2^2)} \left[\frac{h_1 (h_1 + 2h_2)}{(h_1 - h_2)^2} \ln(\frac{h_1}{h_2}) - \frac{5h_1 + h_2}{2(h_1 - h_2)} \right] \tag{2.31}$$

Using Eq. (2.29) and the substitution $H = h_1/h_2$:

$$y_{cp} = \frac{2H(H+2)\ln H - (5H+1)(H-1)}{2(H^2-1)\ln H - 4(H-1)^2} D \tag{2.32}$$

The center of pressure of the film is always more toward the outlet than at the center of the wafer ($y_{cp} > 0.5D$) to produce positive net force and to sustain the normal load. The pressure center will approach the center of the wafer when film thickness ratio, $H = h_1/h_2$, is close but still greater than unity, i.e., the wafer attack angle is positive but very small.

The wafer is free to assume any inclination when supported by a gimbaling point,. Thus, h_1 and h_2 in Eqs. (2.29) and (2.31) are generally unknown, and require two more constraints to determine them. The first constraint is the force equilibrium on the wafer, i.e. the pressure integral per unit width of wafer is equal to the product of the average pressure applied, p_{ave}, and the wafer diameter:

$$f_n = p_{ave} D \tag{2.33}$$

The second constraint is moment equilibrium on the wafer. Because the gimbal cannot sustain any moment, the center of the pressure, y_{cp}, must be located at the given location of the gimbaling point, y^*:

$$y^* = y_{cp} \tag{2.34}$$

The fluid shear at the wafer surface can be written as:

$$\begin{aligned}\tau_{zx} &= \eta \frac{\partial v_y}{\partial z} \\ &= \frac{\eta v_R}{h} + \frac{h}{2}\frac{dp}{dx} = \eta v_R \left(\frac{4}{h} - \frac{3h_o}{h^2}\right)\end{aligned} \tag{2.35}$$

Integrating Eq. (2.35), the frictional force per unit width, f_t , due to fluid shear can be written as:

$$f_t = \frac{\eta v_R D}{(h_1 - h_2)} \left[4 \ln\left(\frac{h_1}{h_2}\right) - \frac{6(h_1 - h_2)}{(h_1 + h_2)} \right] \tag{2.36}$$

From Eqs. (2.33) and (2.36), the friction coefficient in the hydroplaning mode can be obtained:

$$\mu = \frac{f_t}{f_n} = \frac{\eta v_R}{p_{ave}} \frac{1}{(h_1 - h_2)} \left[4 \ln\left(\frac{h_1}{h_2}\right) - \frac{6(h_1 - h_2)}{(h_1 + h_2)} \right] \tag{2.37}$$

From Eq. (2.37), the friction coefficient increases with slurry viscosity η and velocity v_R, and decreases with applied pressure. Equation (2.37) also states that the friction coefficient is a function of h_1 and h_2. However, based on Eqs. (2.33) and (2.34), h_1 and h_2 are not predetermined quantities and will depend on pressure, relative velocity, slurry viscosity, location of gimbaling point and wafer diameter. In practice, the friction coefficient μ can be directly measured and plotted against $\eta v_R/p_{ave}$ to obtain the numerical value of the h_1 and h_2 dependent terms at the right-hand side of Eq. (2.37), which may help determine the geometry of slurry film gap.

In the above analysis, the surfaces of the wafer and the pad are assumed to be smooth. In reality, this will only be true when the film thickness is much larger than the roughness of the pad so that the local topography of the pad surface will not affect the slurry flow. Moreover, a flat wafer surface is also assumed throughout the analysis although the wafer may be slightly curved. However, if the curvature is very small, similar results in terms of frictional force and friction coefficient will be obtained as those of a planar wafer surface (Pinkus and Sternlicht, 1961).

The friction coefficient for a typical CMP process can be estimated based on the above analysis. By assuming that the gimbaling point is much closer to the center of the wafer, the

film thickness at inlet is very close to but larger than that in the outlet, i.e., $h_1 \approx h_2$. Therefore, the numerical value of the terms inside the bracket on the right-hand side of Eq. (2.37) is less than unity. For typical process conditions: η = 0.005 Pa·s, v_R = 0.8 m/s, p = 48 kPa, and y_{cp} = 0.51D, h_1 = 22 µm and h_2 = 19 µm. The friction coefficient μ from Eq. (2.37) is about 0.004. Because most CMP processes operate close to these conditions, a low friction coefficient on the order of 0.001 is expected if the wafer is in the hydroplaning mode.

The volume flow rate of slurry per unit width needed to maintain the fluid film can be calculated by:

$$q_y = \int_0^h v_y dz = -\frac{h^3}{12\eta}\frac{dp}{dy} + \frac{h(u_{y,w} + u_{y,p})}{2} \tag{2.38}$$

Evaluating the flow rate where *(dp/dy)* = 0, Eq. (2.38) reduces to:

$$q_y = \frac{h_o(u_{y,w} + u_{y,p})}{2} \tag{2.39}$$

For typical CMP of 100-mm diameter wafer, the flow rate is about 100 ml/min. If the "side leakage" is taken into account, a higher flow rate is required to maintain hydroplaning.

The above analysis used a simplified one-dimensional model for hydroplaning for calculating the pressure distribution, friction force, friction coefficient, and slurry flow rate. However, as shown earlier in Eq. (2.22), the flow field of the slurry is a complex function of x and y, even if the relative velocity is identical across the wafer. This non-uniform velocity field will introduce nonuniform polishing within the wafer, which will be addressed later.

2.2.5 The Mixed Mode. The friction force at the wafer/pad interface in the mixed mode may be described as the weighted sum of the forces necessary to deform the surface asperities at wafer/pad or wafer/particle contacts and the shear of the viscous slurry film. Thus the frictional force may be written as:

$$F_t = \alpha A \tau_a + \beta A \tau_p + [1-(\alpha+\beta)]A\tau_l \tag{2.40}$$

where τ_a is the shear stress at the wafer/particle contact, τ_p the shear stress at the wafer/pad contact, and τ_l the shear stress in slurry film. The constants α and β represent the fractional area in contact with the abrasive particles and the pad asperities. Therefore, the friction coefficient is expressed as:

$$\mu = \alpha\mu_a + \beta\mu_p + [1-(\alpha+\beta)]\mu_l \tag{2.41}$$

where μ_a is the friction coefficient due to wafer/particle contact, μ_p that due to the wafer/pad contact, and μ_l that due to shear in slurry film. The friction coefficient in the mixed mode will be lower than that in the contact mode, but far higher than that in the hydroplaning mode. The limitation of Eq. (2.41) is that the friction coefficient can only be obtained by experiments since α and β are generally not known *a priori*. In the mixed mode, all the factors that affect the friction coefficient in the contact and hydroplaning modes may have effects.

2.3 Experimental

The polishing experiments used a rotary-type polisher, shown in Fig. 2.4. The stainless steel wafer carrier is connected to a head motor by a gimbaling mechanism to align the wafer parallel to the platen surface. Two load sensors and a torque sensor measure the frictional forces in two orthogonal directions and the torque of the head motor. The capacities of the load and the torque sensors are 222 N and 5.65 N·m, and the resolutions are 0.067 N and 0.001 N·m, respectively. The head unit is driven by pneumatic pistons for vertical motion and for applying normal pressure. The platen unit is a detachable 300-mm diameter aluminum platen and a platen motor. Surfaces of the aluminum platen and the base were ground to achieve a high degree of flatness and surface finish. The polisher is computer controlled so that the applied load and rotational speeds of the wafer carrier and platen can be controlled independently, and the forces and torques on the wafer can be acquired in real

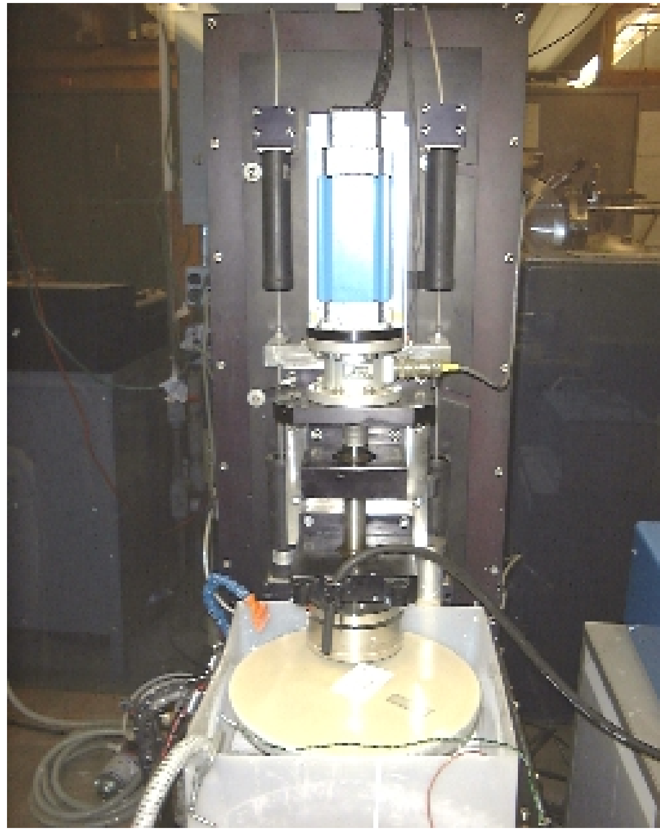

Figure 2.4 Experimental apparatus.

time. The entire apparatus is housed inside a laminar flow module equipped with HEPA filters to ensure a contaminant-free environment.

Silicon wafer substrates, 100 mm in diameter and coated with 20 nm TiN as the adhesion layer and 1-µm PVD Cu on the top, were the test wafers. The density and hardness of the coating materials are listed in Table 2.1. A neutral slurry (pH = 7) with Al_2O_3 abrasive particles was used. The viscosity of the slurry was about 0.03 $\text{Pa} \cdot \text{s}$. Other properties are shown in Table 2.2. The experiments used a commercial composite pad (Rodel IC1400). The pad comprised a microporous polyurethane top layer (Rodel IC1000) and a high-density urethane foam underlayer. The room temperature elastic moduli of the top pad and the composite pad were about 500 MPa and 60 MPa, respectively. Further details of the pad are listed in Table 2.3. Table 2.4 lists the experimental conditions employed in this study.

Each wafer was weighed before and after polishing to calculate the average material removal rate (MRR). The worn pad surface and Cu-coated wafer surfaces were observed in a scanning electron microscope (SEM) to characterize the post-CMP pad topography and surface scratches on wafers.

2.4 Results and Discussion

2.4.1 Friction Coefficient versus the Parameter $\eta v_R/p$. The experimental results are presented in Table 2.5. The friction coefficient (μ), mass loss, volume loss, material removal rate (MRR), the normalized material removal rate (NMRR) and the Preston constant (k_p) are listed for a wide range of velocities and two pressures. The normalized material removal rate is defined as the thickness of material removed per unit distance slid, $d\xi/dS$, where ξ is the thickness removed and S the distance slid (= $v_R t$). Both the MRR ($d\xi/dt$) and the NMRR ($d\xi/dS$) are expressed as the ratios of the variables involved, not as their derivatives.

Figure 2.5 shows the effects of relative velocity and pressure on the friction coefficient. The relative velocities (0.05 to 3.91 m/s) and pressures (14 kPa and 48 kPa) employed in the experiments cover a wide range of practical CMP conditions. The friction coefficient is

Table 2.1: Density and hardness of experimental materials.

Material	Density (kg/m^3)	Hardness (MPa)
Cu	8,920	1,220$\pm$ 50
TiN	5,430	17,640$\pm$ 1,235
Si	2,420	8,776$\pm$ 570

*Hardness values based on the microindentation measurements on thin films.

Table 2.2: Properties of slurry.

Abrasive	α- Al_2O_3
Average Particle Size (μm)	0.3
Particle Hardness (MPa)	20,500
Concentration (vol.%)	2-3
Viscosity (Pa·s)	0.03
pH	7

Table 2.3: Pad properties.

Pad	Rodel IC1400 (k-grooving)
Material	Polyurethane
Thickness (mm)	2.61 (1.27*)
Density (kg/m^3)	750*
Hardness	57 shore D*
Pore Size (μm)	20-60 (isolated)*
Groove Pattern	250 μm wide, 375 μm deep with a 1.5 mm pitch, concentric

* Top pad (IC1000)

Table 2.4: Experimental conditions

Normal Load (N)	108, 379
Normal Pressure (kPa)	14, 48
Angular Speed (rpm)	5 - 420
Linear Velocity (m/s)	0.05 - 3.91
Slurry Flow Rate (ml/min)	150 - 250
Duration (min)	2
Sliding Distance (m)	6 - 469
Ambient Temperature (°C)	22
Relative Humidity (%)	35-45

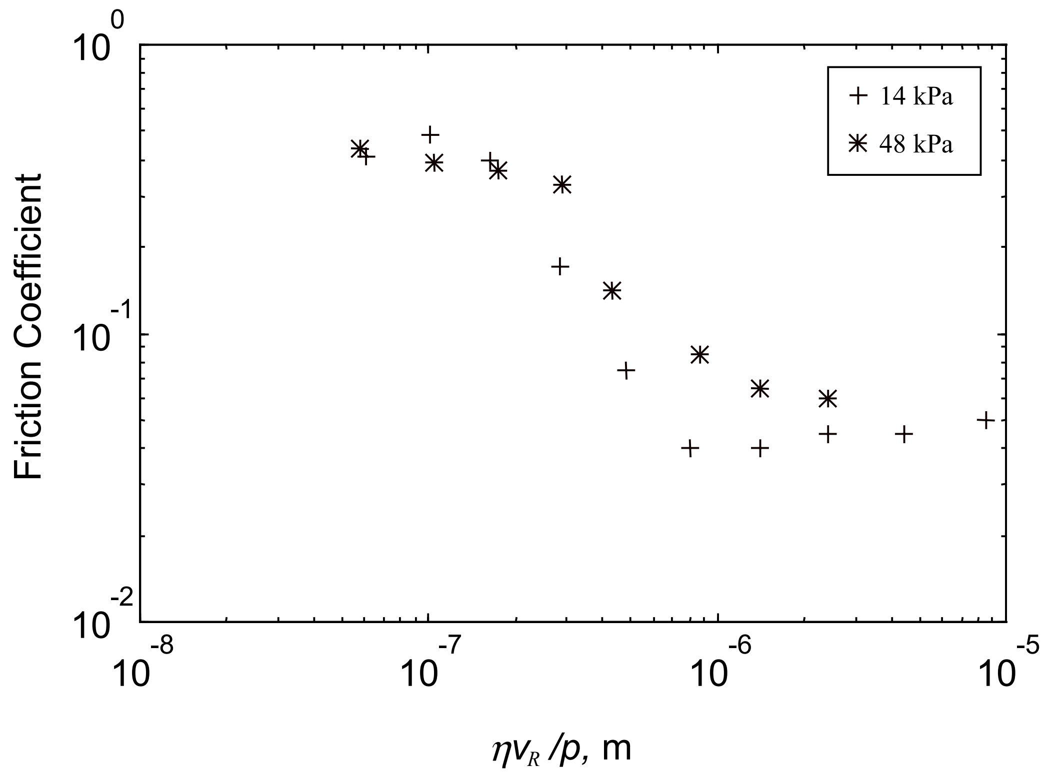

Figure 2.5 The effect of the parameter $\eta v_R / p$ on friction coefficient at the pressure of 14 kPa and of 48 kPa.

plotted in Fig. 2.5 against the parameter $\eta v_R/p$ in Eq. (2.37). When $\eta v_R/p$ is small, i.e., at low velocity or high pressure, the friction coefficient is high and ranges between 0.40 and 0.49. As $\eta v_R/p$ increases, the friction coefficient falls from these values to 0.1 or lower. The transition points for the drop in friction for the two applied pressures are slightly off but are in a narrow range of $\eta v_R/p$. After the transition, the friction coefficient seems to reach a minimum and then gradually increases with $\eta v_R/p$. The low friction coefficient values (especially at 14 kPa) are suspect since the friction force was too small to be measured by the load sensors on the experimental setup.

Nevertheless, the experimental results show a consistent trend between the friction coefficient and the parameter $\eta v_R/p$. For low $\eta v_R/p$ values, the friction coefficient is independent of both the applied pressure and the relative sliding velocity. Thus, the Coulomb friction law is valid. The high friction coefficients in the low $\eta v_R/p$ regime suggest that the wafer/pad interface is in the contact mode. After the transition point, the friction coefficient is no longer independent of pressure or velocity. The friction coefficient decreases with the $\eta v_R/p$. The mixed mode regime sets in and lasts for over an order of magnitude of the $\eta v_R/p$ value. However, the transition point from high to low friction is only slightly affected by the applied pressure. The full-fledged hydrodynamic mode, however, was realized for the experimental conditions chosen because those friction coefficients are far greater than 0.001.

Figure 2.6 presents evidence for wafer/pad contact. It shows the SEM micrographs of the surfaces of a new pad and of a "glazed" pad after polishing 20 blanket wafers at 60 kPa and 0.79 m/s without conditioning. The corresponding value of $\eta v_R/p$ is 0.4×10^{-6} m. A flattened, plastically deformed pad surface with pores clogged by the deformed material is apparent. Such plastic deformation cannot be produced by fluid shear on the pad. Indeed, the flattened surface suggests that the pad had been in contact with the wafer and the high friction force at the wafer/pad deformed the pad surface. Since the wafer surface material, Cu, is much harder than the polyurethane pad, the surface stress may have reached the yield strength of polyurethane and plastically deformed the pad asperities to conform to the flat Cu surface.

2.4.2 Contact versus Hydroplaning. Several researchers (Nakamura et al., 1985; Runnel and Eyman, 1994; Levert et al., 1998; Sundararajan et al., 1999) have reported that

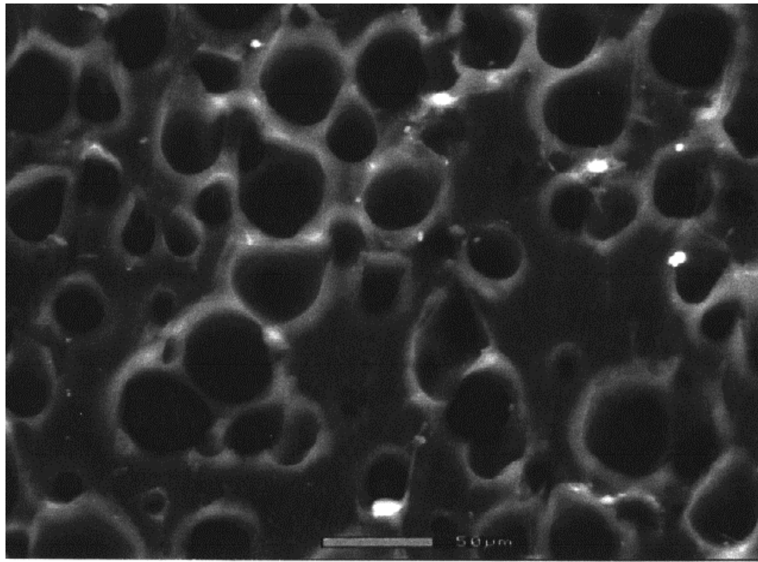

(a)

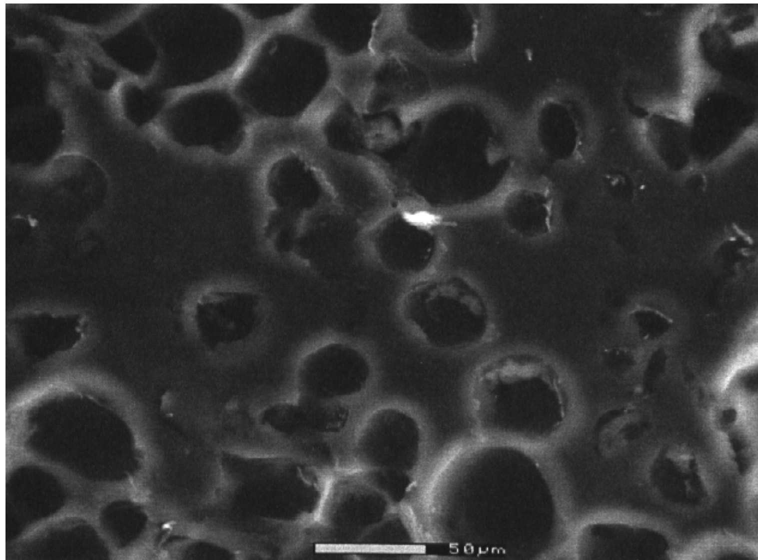

(b)

Figure 2.6 SEM micrographys of pad surfaces: (a) before polishing, and (b) after polishing.

the CMP process operates in the hydroplaning mode. In order to produce a positive pressure gradient at the leading edge of the wafer, they assumed a bowed wafer shape (positive curvature) and numerically solved the Reynolds equation. The estimated film thickness was about 50 μm and the friction coefficient on the order of 0.001. Surprisingly, however, none of the works that claims hydroplaning in CMP has measured the friction coefficient to verify that the process indeed operates in the hydroplaning mode. The present experimental results clearly do not support that the hydroplaning mode prevails even at high velocities up to 3.9 m/s, for even the lowest friction coefficients measured are far greater than 0.001. Indeed, the friction coefficient corresponding to the typical $\eta v_R/p$ values employed in CMP is high and falls in the contact regime.

There are several reasons why it is difficult to achieve hydroplaning in both the linear and rotary CMP machines. (Only the rotary machine will be discussed here, however.) First, even when the angular velocities of the wafer and of the platen are identical so that the relative velocity is unidirectional and uniform over the entire wafer surface, the slurry flow is still two-dimensional. Consequently the one-dimensional analysis, while provides qualitative understanding of the process, is inadequate for designing and operating a CMP machine in the hydroplaning mode. The slurry flow rate should be large enough to compensate for side leakage and to maintain a thick hydrodynamic film from the leading edge to the trailing edge of the wafer. An inadequate supply of the slurry leads to loss of flow continuity and hydrodynamic film, which in turn results in contact or partial contact of the wafer with the pad.

Second, the center of pressure of the hydrodynamic fluid film is not at the center of the wafer, as is evident from the solution of the one-dimensional Reynolds equation. For a plane wafer the pressure center is always located toward the trailing edge of the wafer ($y_{cp} > 0.5D$). Usually, however, the gimbaling point is designed to be above the center of the wafer. Thus, the resultant hydrodynamic force, which will be slightly off-center, produces net moment on the wafer to reduce the attack angle. As the attack angle is reduced, the film collapses, and the normal load cannot be supported by the hydrodynamic film. Thus, all the analyses in the literature set the gimbaling point at the center, and the wafer is assumed to be bowed so that the pressure center coincides with the wafer center. There is no guarantee, however, that the wafers to be polished will always be bowed. In reality, the wafers may have a negative

curvature or even a saddle shape. In these cases, the pressure gradient at the leading edge will be negative so that the fluid film cannot be maintained to sustain the normal load. Moreover, if the two-dimensional flow characteristics of the problem are taken into account, the center of pressure will not be the same as that for the simplified one-dimensional case. It may be extremely sensitive to the velocity and slurry flow rate. Indeed, it is difficult if not impossible to design a rotary CMP machine so that the gimbaling point can always be located at the center of pressure for a range of pressures and velocities. Thus, it is rare for commercial or experimental machines to operate in the hydroplaning mode.

Third, both the one-dimensional and the two-dimensional hydrodynamic analyses assume that the surfaces of the wafer and the pad are rigid and extremely smooth. Clearly, neither of these assumptions are quite correct. However, the wafer may be assumed to be rigid and smooth in comparison with the pad. Film thickness must be greater than three times the composite RMS roughness of the opposing surfaces for hydroplaning to be a viable mode of operation. At smaller scales this requirement may be met for the wafers and pads employed in the CMP practice. On the wafer scale, however, the waviness of the wafer and that of the pad are of interest. Again, if it is assumed that the wafer is flat, the waviness of the pad becomes critical. For a fluid film thickness of about 20-50 μm as calculated earlier, the amplitude of the waviness of the pad should be less than 7-16 μm to sustain the hydrodynamic film. It is unrealistic to expect that commercial polishing pads meet this standard. In fact, if the platen runout is also taken into account, it is quite difficult to operate the CMP machines in the hydrodynamic mode. Any unsteady condition might cause part of the wafer to touch the pad, disrupt the fluid flow, and bring the wafer into the contact mode, or at best into the mixed mode. It may be concluded, therefore, the wafer/pad interface rarely operates in the hydrodynamic mode. At best the contact will be in the mixed mode, as supported by the experimental results shown in Table 5.

2.4.3 Material Removal Rate and the Preston Constant. As suggested by the Preston equation (Eq. (2.1)), Fig. 2.7 shows the material removal rate, MRR, plotted against the product pv_R. Literature data on Cu polishing (Stavreva et al., 1995 & 97; Luo et al., 1998) are also included in the plot. The corresponding conditions are shown in Table 2.6. The present

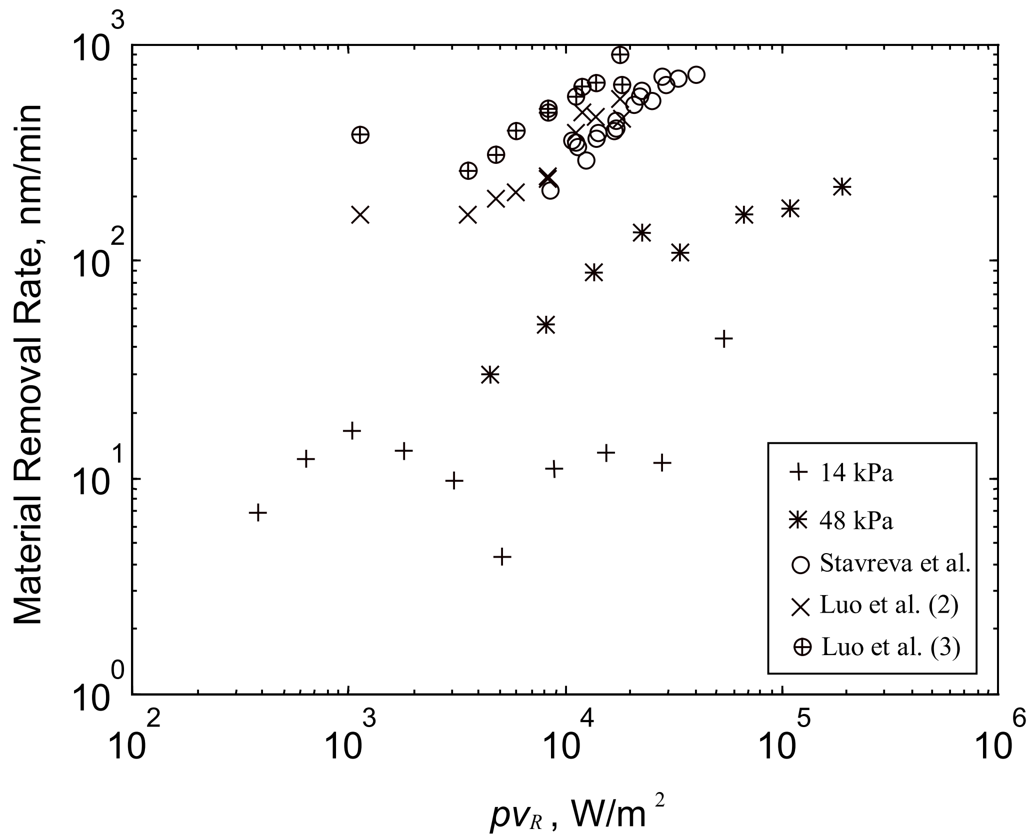

Figure 2.7 The effect of pv_R product (energy flux) on Cu removal rate.

Table 2.6: Experimental conditions among different researchers

Research Group	p (N/m^2)	v_R (m/s)	η (Pa·s)	Pad
M.I.T.	14, 48	0.05 - 3.91	0.03	IC 1400
Stavreva et al. (1995 and 1997)[1]	13 - 30	0.25 - 1.30	0.005[4]	IC 1000 + SUBA IV
Luo et al. (1998)[2],[3]	4 - 66	0.12 - 0.60	0.005[4]	IC 1000 + SUBA IV

(1) SiO_2 based Cu slurry (Rodel XJFW7355 and XJFW8099) diluted with 30 % H_2O_2 (3:1).
(2) SiO_2 based Cu slurry (Rodel QCTT1010) diluted with 30 % H_2O_2 (3:1).
(3) 5 wt.% SiO_2 abrasive with 0.1 M $Fe(NO_3)_3$ and 0.005 M BTA.
(4) Viscosity is assumed based on the data of similar commercial products.

data are obtained with a neutral slurry over a wide range of pv_R values, whereas the literature data represent chemical mechanical polishing but over a narrow range of p and v_R. The mode of contact, however, should not depend on the chemistry of the slurry. Thus, if the mechanism of material removal is not affected by variation in p, v_R, or pv_R, the scatter in the data should be small. The slope of a line drawn through the data points is the Preston constant. The large scatter in the data clearly shows that the Preston constant is indeed not constant. Figure 2.8 shows a plot of the Preston constant versus pv_R for the present experimental data and those obtained from the literature. It is apparent that the data are widely scattered because the wafer/pad interface is not in contact for the majority of the pv_R values.

Thus, to better delineate the effect of contact conditions, the normalized material removal rate, NMRR, and the Preston constant, k_p, is plotted in Figs. 2.9 and 2.10 against the dimensional parameter $\eta v_R/p$ in Eq. (2.37), respectively. The NMRR and Preston constant do not depend on the applied pressure and the velocity when $\eta v_R/p$ is small. It is about 0.2×10^{-6} MPa^{-1} at 14 kPa and 0.1×10^{-6} MPa^{-1} at 48 kPa. The Preston constant stays high at low $\eta v_R/p$, i.e., in the contact mode, and drops down after the critical value, denoted as $(\eta v_R/p)_c$. The experimental results show that the transition occurs around the same $(\eta v_R/p)_c$ for both pressures. This implies that the Preston constant is independent of pressure and velocity when the wafer/pad interface is in the contact mode. After the transition point, the Preston constant decreases as v_R increases or p decreases. The Preston constant shows the same trend as that of friction coefficient, Fig. 2.5, and the transition in k_p occurs at about the same values of $\eta v_R/p$. In the transition regime, the Preston constant is not independent of pressure and velocity. It is found that k_p varies as $(\eta v_R/p)^{-1}$ at 14kPa and as $(\eta v_R/p)^{-0.5}$ at 48 kPa in the mixed regime.

The variation of k_p can be explained in terms of the shifting interfacial conditions. In the mixed mode, the friction coefficient decreases with $\eta v_R/p$. This implies that the wafer/pad contact area also decreases with $\eta v_R/p$. Lack of contact further reduces the material removal rate because the fluid shear and the motion of the loose particles in the discontinuous fluid film cannot apply sufficient pressure on the wafer surface and remove material. With increasing $\eta v_R/p$, particle rolling will increase and particle translation will decrease. In fact,

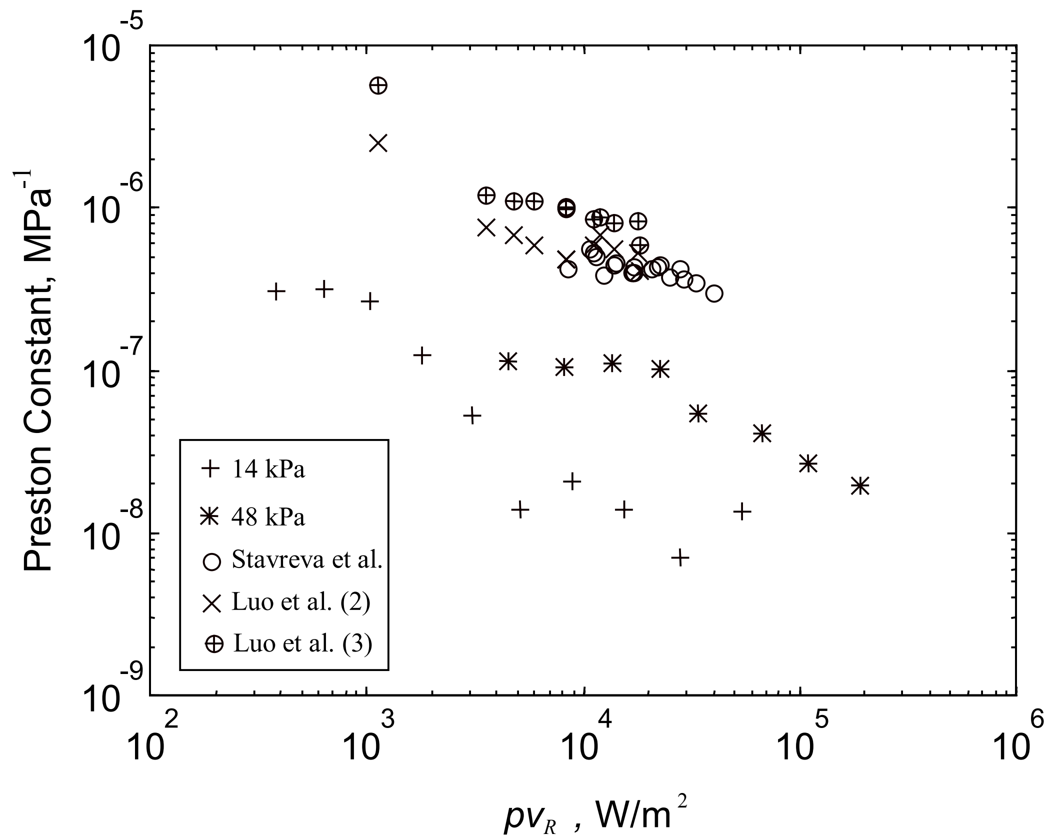

Figure 2.8 The effect of pv_R product (energy flux) on the Preston constant for Cu polishing.

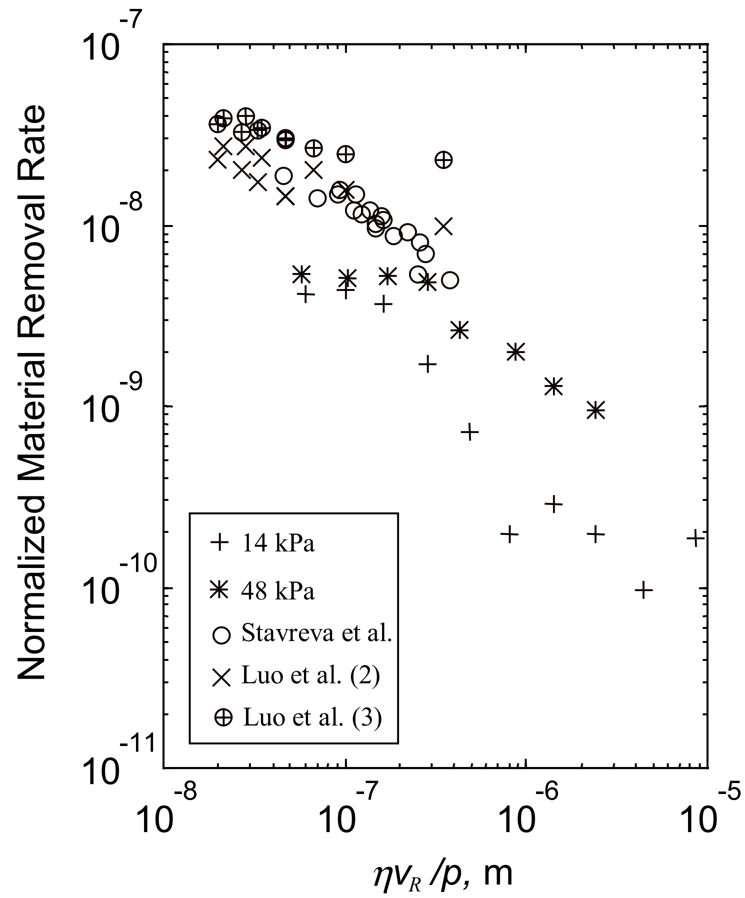

Figure 2.9 The effect of the parameter $\eta v_R / p$ on the normalized material removal rate for Cu polishing.

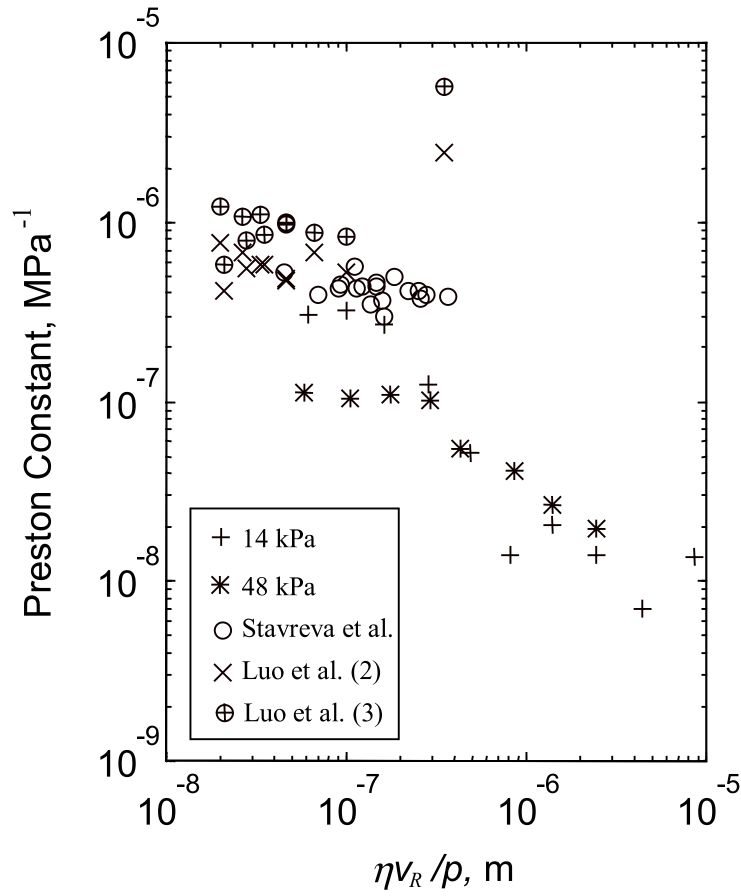

Figure 2.10 The effect of the parameter $\eta v_R / p$ on the Preston constant for Cu polishing.

some researchers tried to fit their data numerically to account for the variation of the Preston "constant" at low pressure or high velocity conditions by a polynomial function of the pv_R product (Zhao and Shi, 1999), or to introduce extra pressure and/or velocity terms to the Preston equation (Luo et al., 1998). They proposed that the interfacial shear stress and particle velocity enhance the chemical reaction rate or mass transfer from the wafer surface. However, the variation in k_p might just be due to the varying interfacial contact modes as Fig. 2.9 shows. Thus each contact mode is expected to have a different Preston constant.

A cross plot of the Preston constant versus friction coefficient is shown in Fig. 2.11. Before the transition point, i.e., at the beginning of the mixed mode, the Preston constant and friction coefficient are positively correlated; the correlation coefficient is almost 1. However, the Preston constant shows less correlation with the friction coefficient with an increase of $\eta v_R/p$ in the mixed mode. Figure 2.10 demonstrates the variation in material removal rates with different contact modes.

2.4.4 Process Optimization. The effects of the parameter $\eta v_R/p$ on the friction coefficient and Preston constant provide an opportunity to optimize the CMP process. For a certain slurry viscosity, the different wafer/pad contact regimes can be delineated in the v_R-p space as shown in Fig. 2.12. Corresponding to the critical point $(\eta v_R/p)_c$ for transition from contact mode to the mixed mode (Fig. 2.5), a line L_1 with the slope $(\eta v_R/p)_c$ is drawn in Fig. 2.12 to represent the transition points for different pressures and velocities. The region bounded by L_1 and the p-axis represents the contact mode. Similarly, another line, L_2, with a greater slope to represent the transition from the mixed mode to the hydroplaning mode is drawn. The region bounded by L_2 and the v_R-axis represents the hydroplaning mode. The region bounded by L_1 and L_2 represents the mixed mode.

Two wafer-scale requirements, material removal rate (MRR) and within-wafer non-uniformity (WIWNU), should be simultaneously satisfied for CMP process optimization. A high Preston constant regime should be chosen for high MRR. This corresponds to the contact regime below line L_1 in Fig. 2.12, where the Preston constant is high and independent of both p and v_R. From the viewpoint of reducing WIWNU, the contact mode is preferable

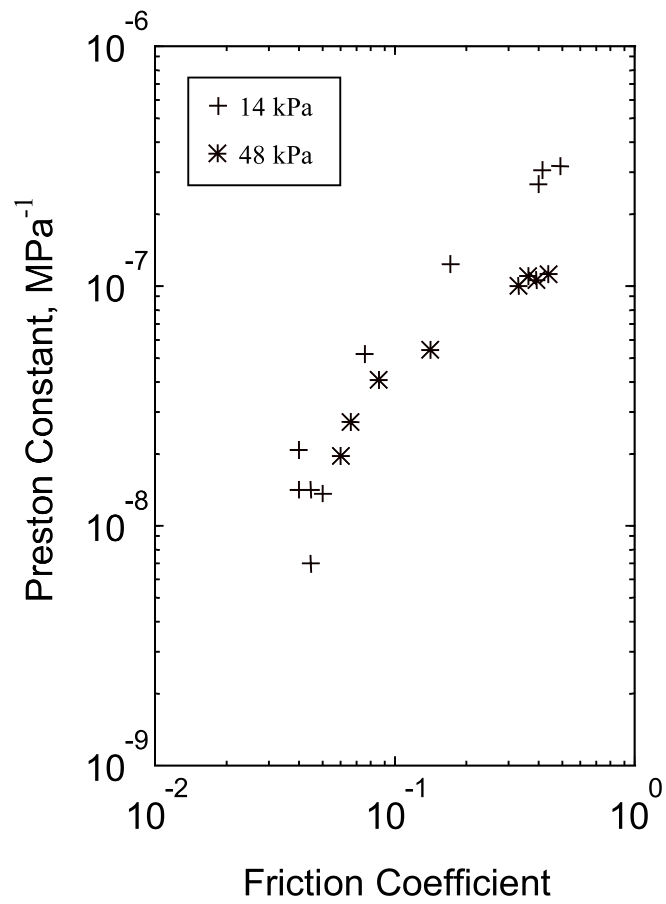

Figure 2.11 The correlation between the Preston constant and the friction coefficient.

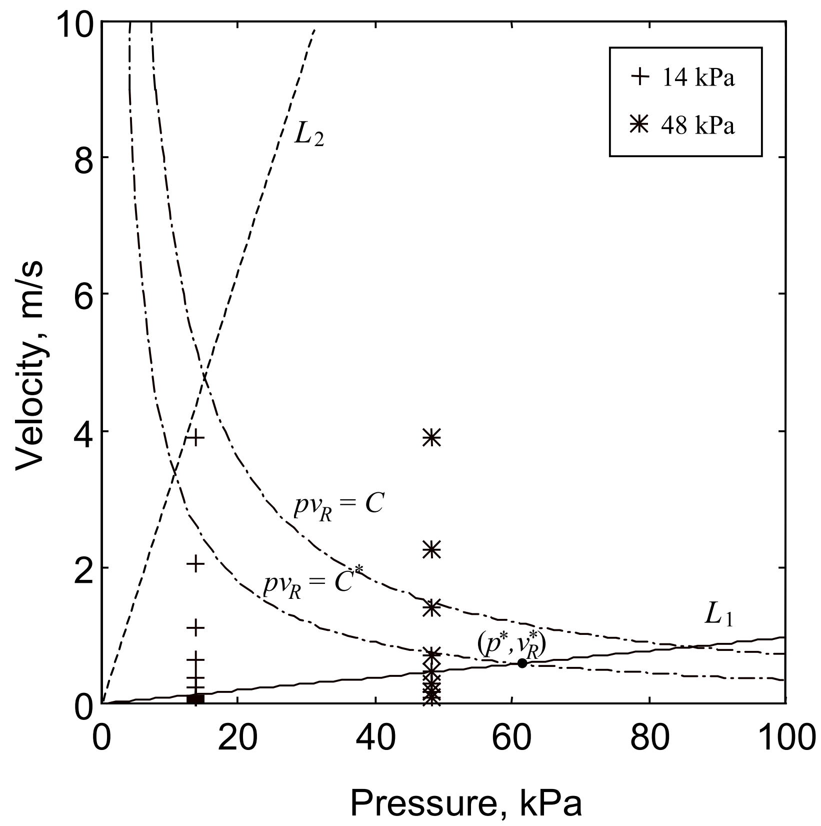

Figure 2.12 Schematic of process optimization.

with $\omega_w = \omega_p$ because the wafer/pad contact interface is more stable than the hydroplaning mode or the mixed mode and the velocity is uniform over the entire surface of the wafer.

From Eq. (2.1), the pv_R product should be as high as possible to increase the MRR, i.e., the highest velocity available is preferable in the contact regime for a given pressure and vice versa. This suggests that the optimal conditions are located on the line L_1. However, a high pressure requires a sturdy machine structure, which generally sets an upper limit for the applicable pressure. In addition, even a small vibration of the machine at high pressure might result in large fluctuations on the normal load and friction force at the wafer/pad contact interface, and thus increase the WIWNU. These considerations suggest that the pressure increase cannot be unlimited. Similarly, extremely high velocities are not desirable because it is difficult to retain the fluid slurry on the platen at high velocities.

Even a more important consideration for the choice of pressure and velocity is that of heat generation. The rate of thermal energy generation due to friction, P, can be expressed as

$$P = \mu \pi r_W^2 p v_R \tag{2.42}$$

The higher the value of the product pv_R is, the more the heat generation rate is. The typical value of heat generation rate for a 100-mm diameter Cu wafer polished at 48 kPa normal pressure and a velocity of 0.5 m/s is about 80 W. The frictional heat will raise temperature and vary the chemical reaction rates locally and thus deteriorate polishing uniformity. In the contact mode, the heat generated might not be efficiently removed by the slurry transport because the volume flow rate through the interface is rather low. Even with external cooling of the pad and the wafer carrier, the heat removal rate could still be limited due to the low thermal conductivities of the silicon wafer and the polyurethane pad. Thus an upper limit for the applicable pv_R product can be set as $pv_R = C$, where C is a constant that depends on the friction coefficient, geometry, and the thermal properties of the polishing head, platen, pad, and so on. The constraint $pv_R = C$ is shown as a rectangular hyperbola in Fig. 2.12. The optimal process condition (p^*, v_R^*) is defined by the intersection of $pv_R = C$ with L_1. Operation of the CMP process in the mixed and hydrodynamic modes is not optimum for reasons cited earlier. In practice, appropriate external cooling may be installed in the

polishing head and the platen to improve the efficiency of heat removal and increase the constant C. Thus a higher MRR can be achieved by increasing the optimal $p^* v_R^*$ product. For other practical reasons (such as mechanical vibration, slurry retainment), however, the optimal pressure and velocities could be somewhat different from p^* and v_R^*. Thus the friction force measurements during CMP could be effectively used, according to Eq. (2.42), to characterize the process regime, identify the transition point from contact mode to mixed mode, and determine the optimal pressures and velocities for process optimization.

2.5 Conclusions

Three wafer/pad contact conditions, contact, hydroplaning, and mixed modes, were proposed for the CMP process. Models for identifying each mode based on the friction coefficient were formulated. The friction coefficient varied by one or two orders magnitudes among the different contact modes because the resistance to wafer motion can change by orders of magnitude in the presence of a thin slurry film. Typically, the friction coefficient for contact mode is on the order of 0.1, for mixed mode on the order of 0.01 to 0.1, and for full-fledged hydrodynamic mode it will be 0.001. This wide range in friction suggests that friction coefficient can be used as an effective indicator to monitor the contact conditions in the CMP process.

Experiments on Cu blanket wafers with neutral Al_2O_3 slurry were conducted to verify the models for a wide range of pressure and velocity settings. The results suggest that the CMP process must be operated in the contact mode. Hydroplaning is not a stable process mode in terms of the gimbaling point location, wafer curvature, and fluctuations in slurry flow. Accordingly, the important issue in CMP process design is to select process parameters to maintain the process in the stable contact regime.

The effects of process parameters on the material removal rate and the relations between the friction coefficient and the Preston constant were examined. The results show that the Preston constant is only independent of the pressure and velocity in the contact regime. Moreover, the high correlation between the friction coefficient and the Preston constant in the

contact mode suggests the possibility of using friction coefficient to monitor the material removal rate in CMP. Further study on the polishing mechanisms and the role of chemistry in CMP is required to determine the correlation between the friction coefficient and the Preston constant and the material removal rates.

Nomenclature

A = apparent area of wafer (m^2)
D = diameter of the wafer (m)
F_n, F_t = normal and tangential forces on wafer (N)
F_x, F_y = x and y components of friction force (N)
f_n, f_t = normal and tangential forces per unit width (N/m)
H = ratio of inlet and outlet slurry film thicknesses = h_1/h_2
h = slurry film thickness (m)
h_o = characteristic slurry film thickness (m)
h_1, h_2 = slurry film thicknesses at the inlet and outlet of wafer/pad interface (m)
k_p = Preston constant (m^2/N)
L = normal load on wafer (N)
P = the rate of thermal energy generation due to friction (W)
p = normal pressure on wafer (N/m^2)
p^* = optimal normal pressure (N/m^2)
p_{ave} = nominal pressure on wafer(N/m^2)
Q_p, Q_w = torques exerted on pad and wafer
q_y = slurry volume flow rate per unit width (m^2/s)
r, θ = polar coordinates
r_{cc} = distance between the centers of the wafer and the pad (m)
r_p, r_w = distances between a given point on the wafer and the centers of the pad and the wafer (m)
$u_{x,p}$, $u_{y,p}$, $u_{z,p}$ = the x- , y-, and z -direction velocity components of the pad (m/s)
$u_{x,w}$,$u_{y,w}$, $u_{z,w}$ = the x- , y-, and z -direction velocity components of the wafer (m/s)
v_R^* = optimal relative velocity (m/s)
v_R = magnitude of the relative velocity (m/s)
v_r, v_θ = the velocity components in the r, θ coordinates (m/s)
$\bar{v}_{r,R}$, $\bar{v}_{\theta,R}$ = magnitude of components of average relative velocity in r, θ directions (m/s)
v_y = two-dimensional velocity field of the slurry film (m/s)
x, y, z = Cartesian coordinates
y_{cp} = location of the pressure center in the y direction
α, β = weight factors
ω_p, ω_w = angular velocities of the pad and the wafer (rad/s)
η = viscosity of the slurry (Pa·s)
μ = Coulomb friction coefficient
μ_a, μ_l, μ_p = friction coefficients
τ_a, τ_l, τ_p = shear stresses (N/m^2)
τ_{zx} = fluid shear stress on wafer (N/m^2)
ξ = thickness of the material removed on wafer surface (m)

References

Bhushan, M., Rouse, R., and Lukens, J.E., 1995, "Chemical-Mechanical Polishing in Semidirect Contact Mode," *J. Electrochem. Soc.*, Vol. 142, pp. 3845-3851.

Bramono, D.P.Y., and Racz, L.M., 1998, "Numerical Flow-Visulization of Slurry in a Chemical Mechanical Planarization Process," *Proc. 1998 CMP-MIC Conf.*, pp. 185-192.

Brown, N.J., Baker, P.C., and Maney, R.T., 1981, "Optical Polishing of Metals," *Proc. SPIE*, Vol. 306, pp. 42-57.

Bulsara, V.H., Ahn, Y., Chandrasekar, S., Farris, T.N., 1998, "Mechanics of Polishing," ASME *Journal of Applied Mechanics*, Vol. 65, pp. 410-416.

Chekina, O.G., Keer, L.M., and Liang, H., 1998, "Wear-Contact Problems and Modeling of Chemical Mechanical Polishing," *J. Electrochem. Soc.*, Vol. 145, pp. 2100-2106.

Cook, L.M., 1990, "Chemical Processes in Glass Polishing," *J. Non-Crystalline Solids*, Vol. 120, pp. 152-171.

Cook, L.M., Wang, F., James, D.B., and Sethuraman, A.B., 1995, "Theoretical and Practical Aspects of Dielectric and Metal Polishing," *Semiconductor International*, Vol. 18, pp. 141-144.

Coppeta, J., Racz, L., Philipossian, A., Kaufman, F., and Rogers, C., 1998, "Pad Effects on Slurry Transport Beneath a Wafer During Polishing," *Proc. 1998 CMP-MIC Conf.*, pp. 36-43.

Gutmann, R.J., Steigerwald, J.M., You, L., Price, D.T., Neiynck, J., Duguette, D.J., and Murarka, S.P., 1995, "Chemical-Mechanical Polishing of Copper with Oxide and Polymer interlevel Dielectrics," *Thin Solid Films*, Vol. 270, pp. 596-600.

Hamrock, B.J., 1994, *Fundamentals of Fluid Film Lubrication*, McGraw-Hill, New York, pp. 141-186.

Komanduri, R., Umehara, N., and Raghanandan, M., 1996, "On the Possibility of Chemo-Mechanical Action in Magnetic Float Polishing of Silicon Nitride,"ASME*, Journal of Tribology*, Vol. 118, pp. 721-727.

Kaufman, F.B., Thompson, D.B., Broadie, R.E., Jaso, M.A., Guthrie, W.L., Pearson, D.J., and Small, M.B., 1991, "Chemical-Mechanical Polishing for Fabricating Patterned W Metal Features as Chip Interconnects," *J. Electrochem. Soc.*, Vol. 138, pp. 3460-3464.

Landis, H., Burke, P., Cote, W., Hill, W., Hoffman, C., Kaanta, C., Koburger, C., Lange, W., Leach, M., Luce, S., 1992, "Intergration of Chemical-Mechanical Polishing into CMOS Integrated Circuit Manufacturing," *Thin Solid Films*, Vol. 220. pp. 1-7

Liang, H., Kaufman, F., Sevilla, R., and Anjur, S., 1997, "Wear Phenomena in Chemical Mechanical Polishing," *Wear*, Vol. 211, pp. 271-278.

Liu, C.-W., Dai, B.-T., Tseng, W.-T., and Yeh, C.-F., 1996, "Modeling of the Wear Mechanism during Chemical-Mechanical Polishing," *J. Electrochem. Soc.*, Vol. 143, pp. 716-721.

Levert, J.A., Mess, F.M., Salant, R.F., Danyluk, S., and Baker, A.R., 1998, "Mechanisms of Chemical-Mechanical Polishing of SiO_2 Dielectric on integrated Circuits," *Tribology Trans.*, Vol. 41, pp. 593-599.

Luo, Q., Ramarajan, S., and Babu, S.V., 1998, "Modification of Preston Equation for the Chemical-Mechanical Polishing of Copper," *Thin Solid Films*, Vol. 335, pp. 160-167.

Mess, F., Levert, J., and Danyluk, S., 1997, "Vertical Differential Displacements at a Pad/ Sapphire Interface during Polishing," *Wear*, Vol. 211, pp. 311-315.

Nakamura, T., Akamatsu, K., and Arakawa, N., 1985, "A Bowl Feed and Double Sides Polishing for Silicon Wafer for VLSI*," Bulletin Japan Soc. Precision Engg.*, Vol. 19, pp. 120-125.

Patrick, W.J., Guthrie, W.L., Standley, C.L., and Schiable, P.M., 1991, "Application of Chemical Mechanical Polishing to the Fabrication of VLSI Circuit Interconnects," *J. Electrochem. Soc.*, Vol. 138, pp. 1778-1784.

Peters, L., 1998, "Pursuing the Perfect Low-k Dielectric," *Semiconductor International*, Vol. 21, pp. 64-74.

Pinkus, O., and Sternlicht, B., 1961, *Theory of Hydrodynamic Lubrication*, McGraw-Hill, New York.

Preston, F.W., 1927, "The Theory and Design of Plate Glass Polishing Machines," *J. Soc Glass Technology* , Vol. 11, pp. 214-256.

Runnels, S.R., 1994, "Feature-Scale Fluid-Based Erosion Modeling for Chemical-Mechanical Polishing," *J. Electrochem. Soc.*, Vol. 141, pp. 1900-1904.

Runnel, S.R., and Eyman, L.M., 1994, "Tribology Analysis of Chemical-Mechanical Polishing," *J. Electrochem. Soc.*, Vol. 141, pp. 1698-1701.

Runnels, S.R., Kim, I., Schleuter, J., Karlsrud, C., and Desai, M., 1998, "A Modeling Tool for Chemical-Mechanical Polishing Design and Evaluation," *IEEE Tran. on Semiconductor Mfg.*, Vol. 11, pp. 501-510.

Stavreva, Z., Zeidler, D., Plötner, M., Drescher, K., 1995, "Chemical Mechanical Polishing of Copper for Multilevel Metallization," *Appl. Surface Sci.*, Vol. 91, pp. 192-196.

Stavreva, Z., Zeidler, D., Plötner, M., Grasshoff, G., Drescher, K., 1997, "Chemical-Mechanical Polishing of Copper for Interconnect Formation," *Microelectronic Engr.*, Vol. 33, pp. 249-257.

Steigerwald, J.M., Zirpoli, R., Murarka, S.P., Price, D., Gutmann, R.J., 1994, "Pattern Geometry Effects in the Chemical-Mechanical Polishing of Inlaid Copper Structures," *J. Electrochem. Soc.*, Vol. 141, pp. 2842-2848.

Sundararajan, S., Thakurta, D.G., Schwendeman, D.W., Murarka, S.P., and Gill, W.N., 1999, "Two-Dimensional Wafer-Sacle Chemical Mechanical Planarization Models Based on Lubrication Theory and Mass Transport," *J. Electrochem. Soc.*, Vol. 146, pp. 761-766.

Yu, T.-K., Yu, C.C., and Orlowski, M., 1993, "A Statistical Polishing Pad Model for Chemical-Mechanical Polishing," *Proc. 1993 IEEE Int. Electron Dev. Mfg.*, pp. 865-868.

Zhao, B., and Shi, F.G., 1999, "Chemical Mechanical Polishing in IC Process: New Fundamental Insights," *Proc. 1999 CMP-MIC Conf.*, pp. 13-22.